Electronic Supplementary Material (ESI) for Sustainable Energy & Fuels.

Electronic Supplementary Material for

Conductive Co-Based Metal Organic Framework Nanostructures for Excellent Potassium- and Lithium-Ion Storage: Kinetics and Mechanism Studies

Pengcheng Mao,[a] Huilin Fan,[a] Chang Liu,[a] Gongxu Lan,[a] Wei Huang,[b] Zhipeng Li,[c, *] Hitham Mahmoud,[d, e, *] Runguo Zheng,[a, f, g] Zhiyuan Wang,[a, f, g] Hongyu Sun,[f, *] Yanguo Liu [a, f, g, *]

[a] *School of Materials Science and Engineering, Northeastern University, Shenyang 110004, PR China*

[b] *School of Chemistry and Materials Science, Hunan Agricultural University, Changsha 410128, PR China*

[c] *Beijing Advanced Innovation Center for Materials Genome Engineering, School of Materials Science and Engineering, University of Science and Technology Beijing, Beijing 100083, PR China*

[d] *Else Kooi Laboratory, Faculty of Electrical Engineering, Mathematics and Computer Science, Delft University of Technology, Feldmannweg 17, 2628 CT Delft, The Netherlands*

[e] *Chemistry Department, Faculty of Science, Zagazig University, Alsharkia 44519, Egypt*

[f] *School of Resources and Materials, Northeastern University at Qinhuangdao, Qinhuangdao 066004, PR China*

[g] *Key Laboratory of Dielectric and Electrolyte Functional Material Hebei Province, Northeastern University at Qinhuangdao, Qinhuangdao 066004, PR China*

* Corresponding authors. E-mail addresses: hyltsun@gmail.com (H. Sun), lyg@neuq.edu.cn (Y. Liu), H.M.AminHassan@tudelft.nl (H. Mahmoud), zplmse@ustb.edu.cn (Z. Li)

1. Experimental section

1.1. Materials synthesis

Ethanol, HHTP, and cobalt acetate tetrahydrate ($Co(OAc)_2 \cdot 4H_2O$) were purchased from Aladdin Reagent Co., Ltd. The electrolytes used for PIBs and LIBs were provided by Suzhou Duoduo Technology Co., Ltd. The above reagents were used directly without further purification. Co-CAT MOF was prepared by a simple solution phase method.[41] Generally, $Co(OAc)_2 \cdot 4H_2O$ (150 mg) and HHTP (105 mg) were added in deionized water (50 mL) and subjected to sonicate for 30 min. The mixture was transferred into an oil bath pot heated at 85 ℃ for 24 h. The precipitation was collected and washed three times with deionized water and anhydrous ethanol, and then dried at 85 ℃ for 12 h in a vacuum oven.

1.2. Samples characterization

The crystal structures were identified with X-ray diffraction (XRD, Rigaku Smart Lab). The morphology and microstructure were characterized by scanning electron microscopy (SEM, Zeiss SUPRA55 SAPPHIRE, 15 kV) and transmission electron microscopy (TEM, JEOL JEM 2100, 200 kV). The surface valence state analysis was carried out with an X-ray photoelectron spectrometer (XPS, Thermo ESCALAB 250XI). Surface functional groups were probed by Fourier transform infrared spectroscopy (FTIR, Shimadzu FTIR-8400S, 4000 – 400 cm^{-1}) and Raman spectroscopy (LabRAM ARAMIS, 532nm). Porosity and specific surface area were measured by Brunauer-Emmett-Teller (BET) method. Thermogravimetric analysis (TGA, Setsy Evolution) was tested in air atmosphere with a heating rate of 5 ℃ min^{-1}.

1.3. Electrochemical measurements

The electrochemical performance was measured by using CR2032 type coin cells. The working electrodes were fabricated by blending Co-CAT MOF, conductive carbon black and sodium carboxymethyl cellulose with a weight ratio of 7: 2: 1 in deionized water. After stirring for 3 h, the slurry was uniformly coated on a Cu foil, with an average coating amount of ~ 0.45 mg cm^{-2}. The coated copper foil was dried at 80 °C for 8 h in air, and then dried at 120 °C for 8 h under vacuum. To measure the PIB performance, a piece of potassium foil was used as the counter electrode as well as the reference electrode, a glass fiber and ether-based solution (3 M potassium bis(fluorosulfonyl)amide in 1 L 1,2-dimethoxyethane) were used as the separator and the electrolyte, respectively. For LIB measurements, Li metal was used as the counter/reference electrode, and Celgard 2500 membrane was used as the separator. The electrolyte was made by dissolving 1 M $LiPF_6$ in a mixture of ethylene methyl carbonate, ethylene carbonate, and dimethyl carbonate with a volume ratio of 1:1:1. When assembling the full cells, $LiCoO_2$ material was used as cathode, the working electrode was made by blending $LiCoO_2$, conductive carbon black and PVDF with a weight ratio of 90: 5: 5 in N-methylpyrrolidone. The half cells and full cells were assembled in an Ar-filled glove box (the concentrations of water and oxygen were both less than 0.1 ppm). The galvanostatic cycling measurements were conducted between 0.01 and 3.0 V (vs. K^+/K, or Li^+/Li) on a battery test tester (LAND CT2001A). Cyclic voltammograms (CV) were obtained using an electrochemical workstation (CHI660D). Electrochemical impedance spectroscopy (EIS) with the frequency ranging from 100 kHz to 10 mHz and an AC signal of 5 mV in amplitude was taken by a Solartron 1260 + 1287 (UK).

2. Supplementary figures

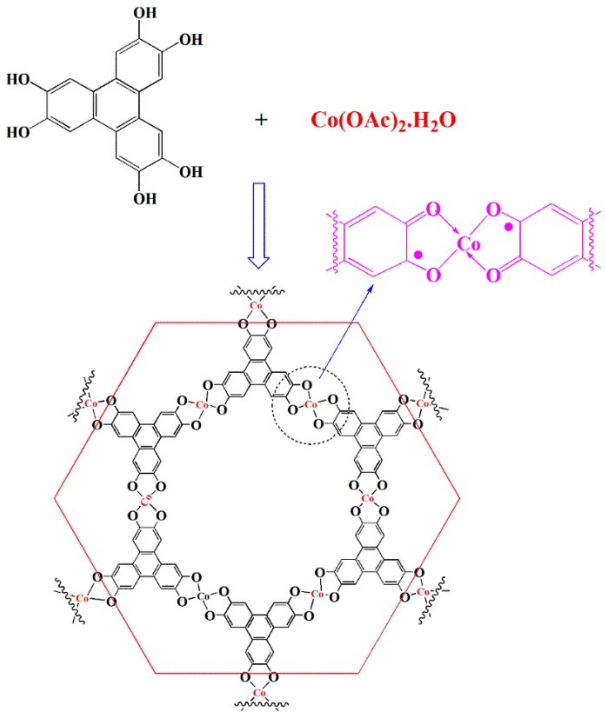

Scheme S1. Scheme showing the synthesis of Co-CAT MOF.

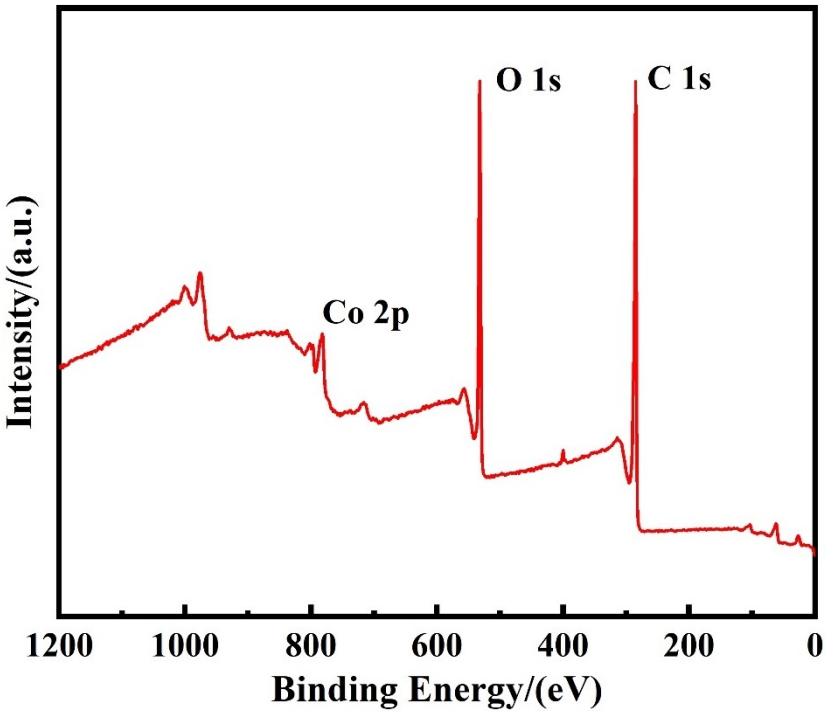

Figure S1. Overall XPS survey spectrum of Co-CAT MOF.

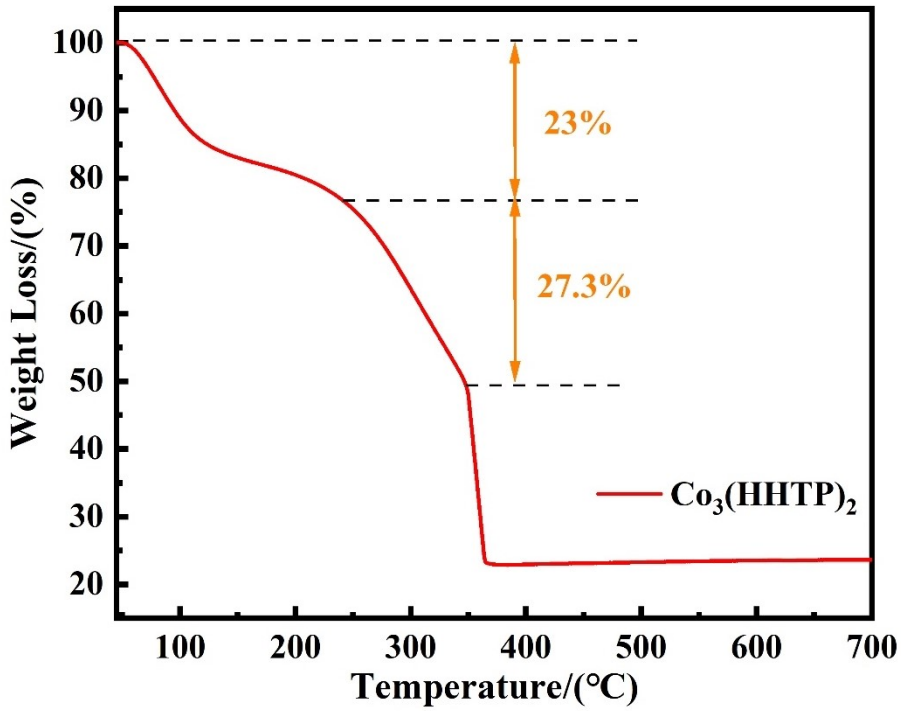

Figure S2. TGA curve of the as-synthesized Co-CAT MOF.

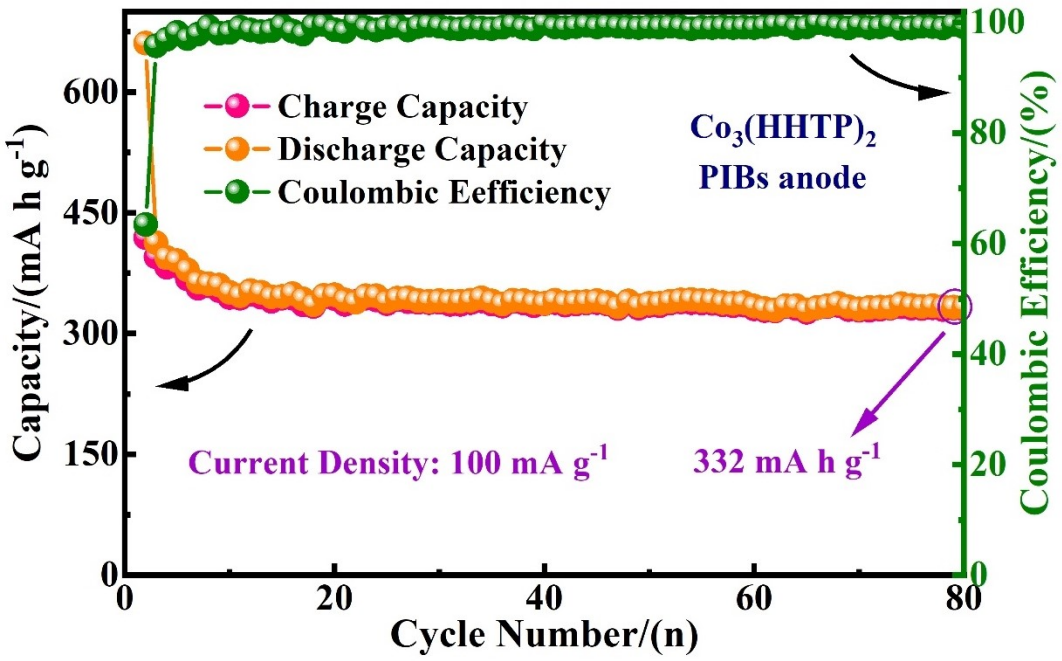

Figure S3. The discharge and charge capacities and corresponding Coulombic efficiencies of Co-CAT MOF anode with the current density of 100 mA g^{-1} over 80 cycles.

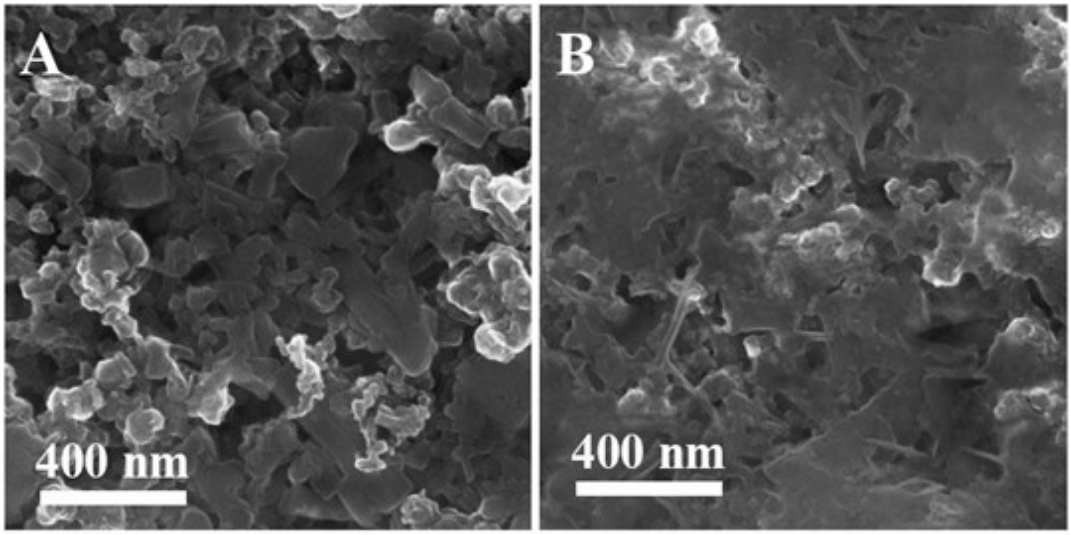

Figure S4. SEM images of (A) fresh Co-CAT MOF electrode and (B) Co-CAT MOF electrode for PIBs after testing at 100 mA g^{-1} for 80 cycles.

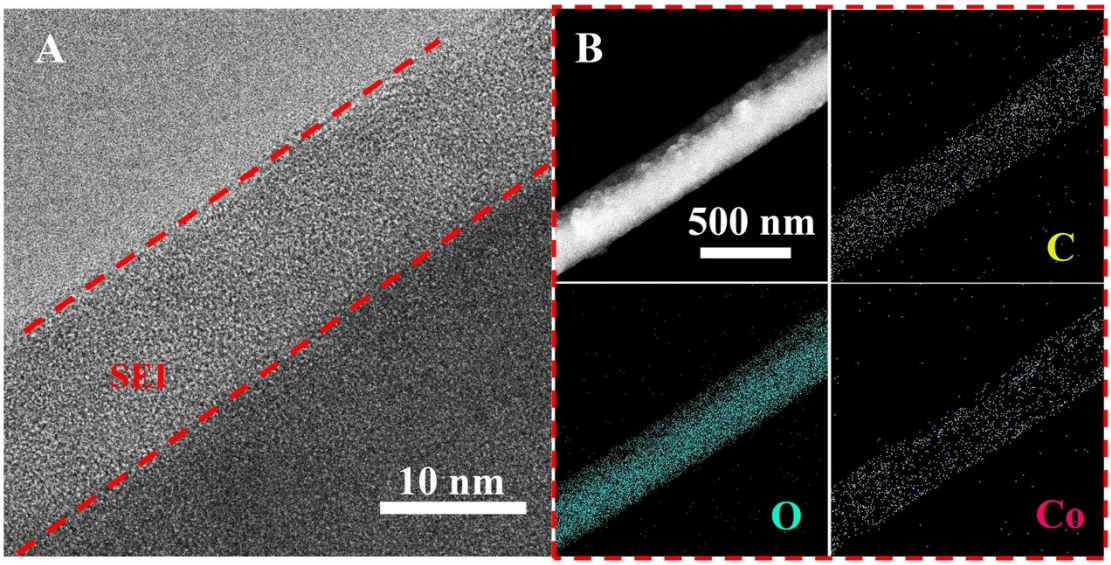

Figure S5. (A) TEM, (B) HAADF-STEM images, and EDX mapping of C, O and Co elements of the cycled Co-CAT MOF for PIB anodes.

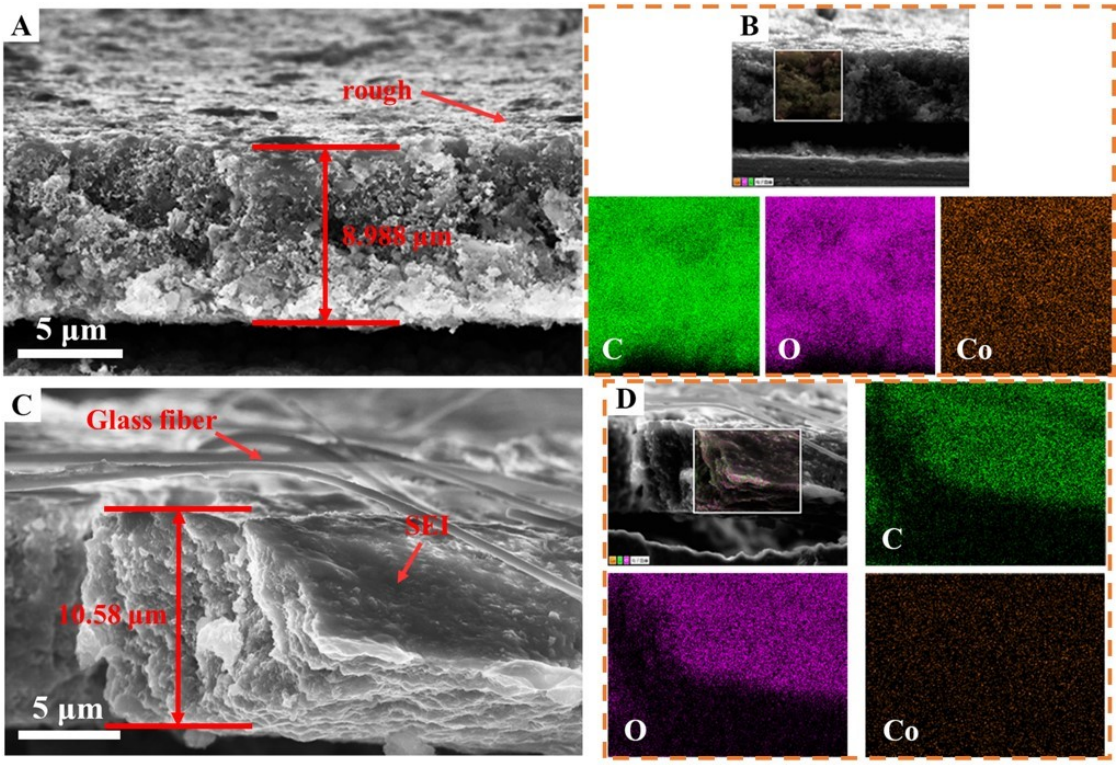

Figure S6. Cross-sectional SEM images and EDX elemental mapping of (A, B) initial electrode and (C, D) cycled Co-CAT MOF for PIB anodes.

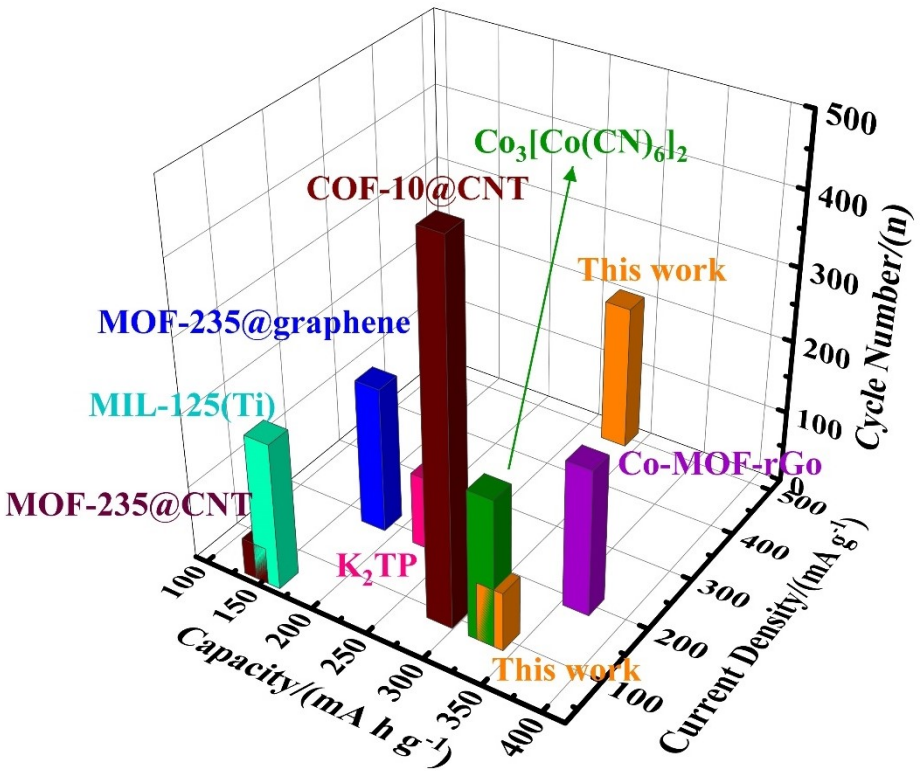

Figure S7. Bar chart of electrochemical performance comparison of MOF-based anodes for PIBs.

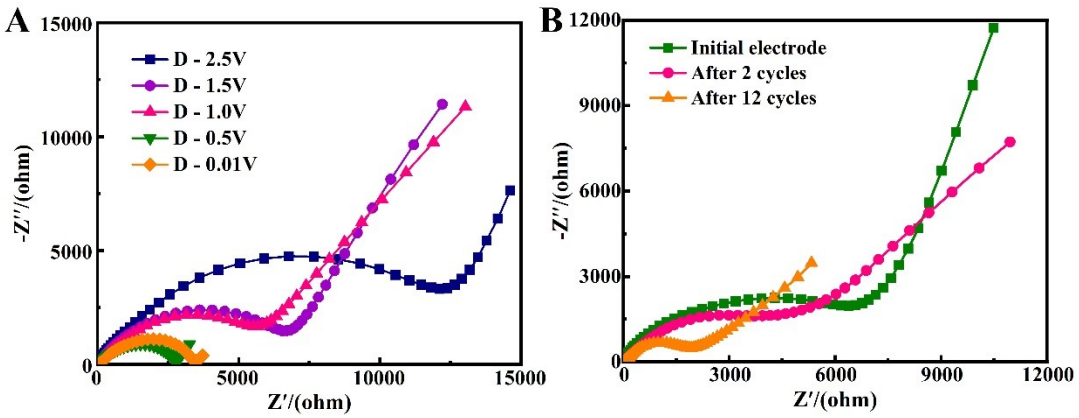

Figure S8. (A) EIS profiles of the Co-CAT MOF electrode measured at different depths of discharge during the first discharging. (B) EIS profiles of the fresh Co-CAT MOF electrode, and the electrode after 2 and 12 charge/discharge cycles.

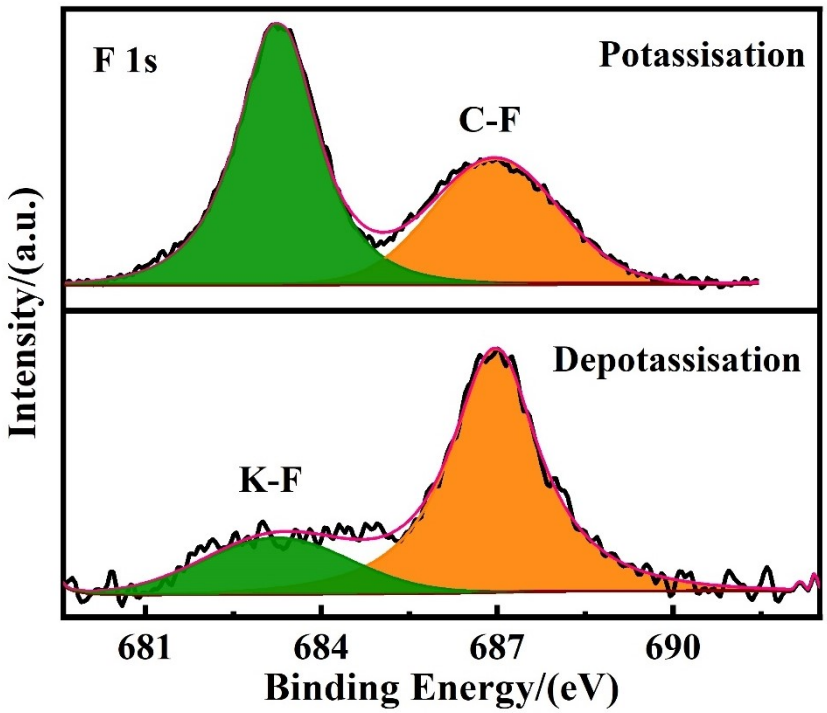

Figure S9. High-resolution XPS spectra of F 1s core level.

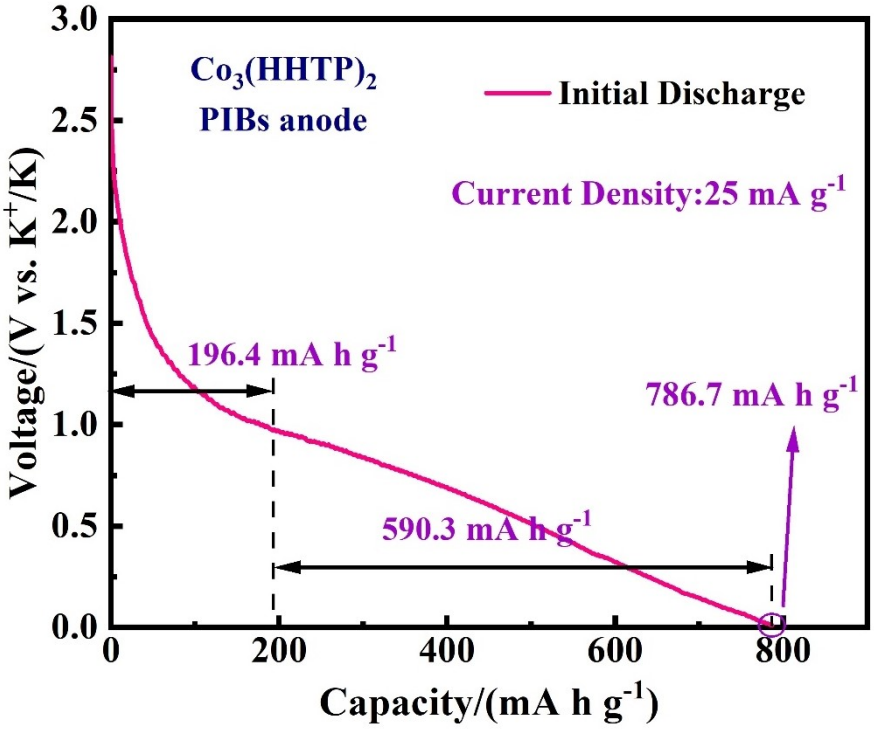

Figure S10. The initial discharge profile for Co-CAT MOF measured at 25 mA g^{-1}.

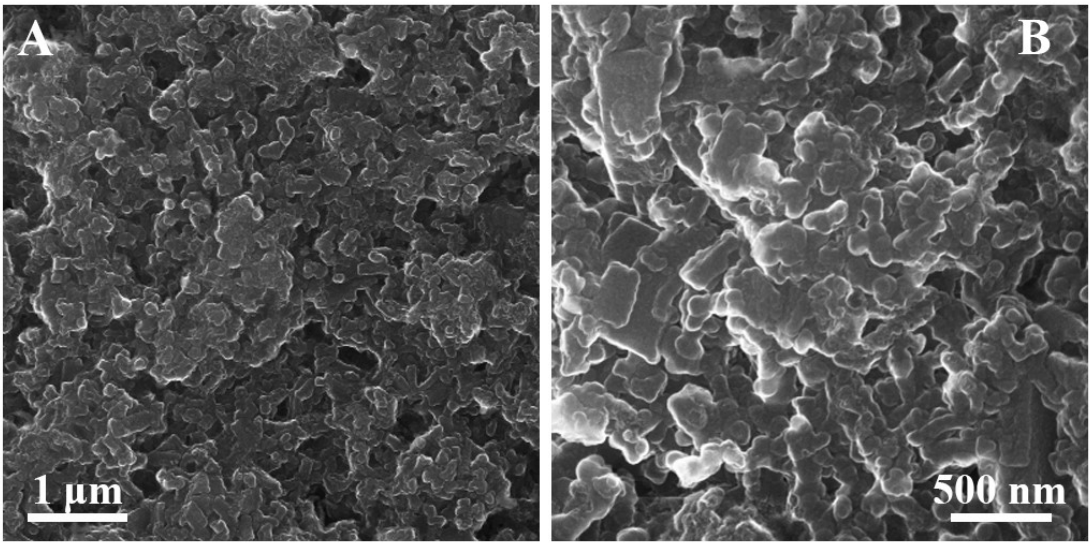

Figure S11. SEM images of the Co-CAT MOF electrode for LIBs after 200 cycles at 200 mA g^{-1}.

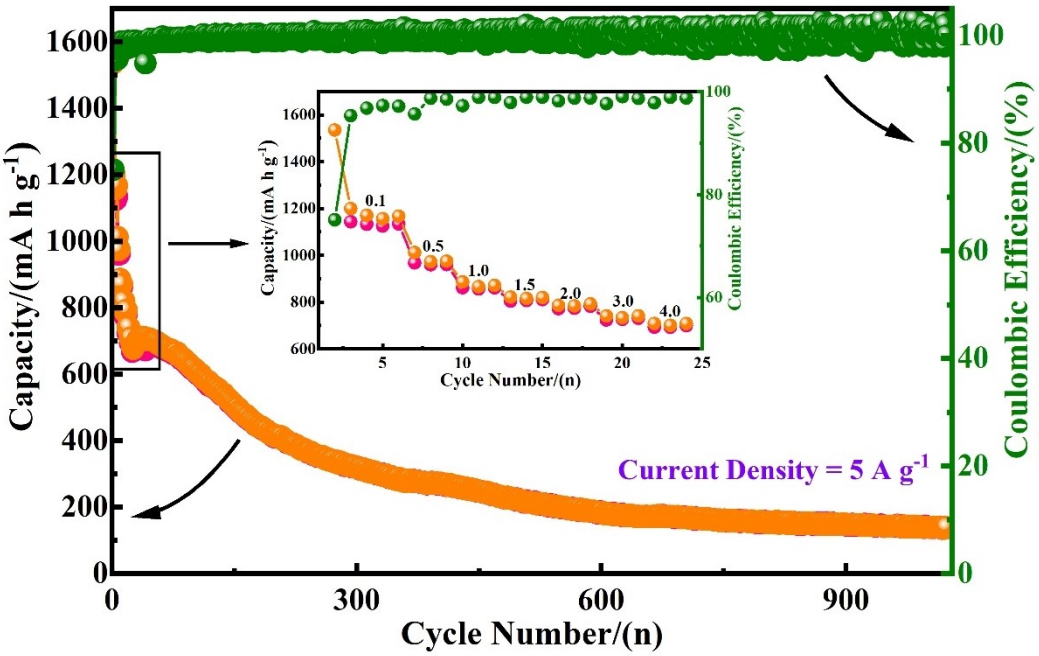

Figure S12. Cycle performance of Co-CAT MOF anode for LIBs measured at 5 A g^{-1}.

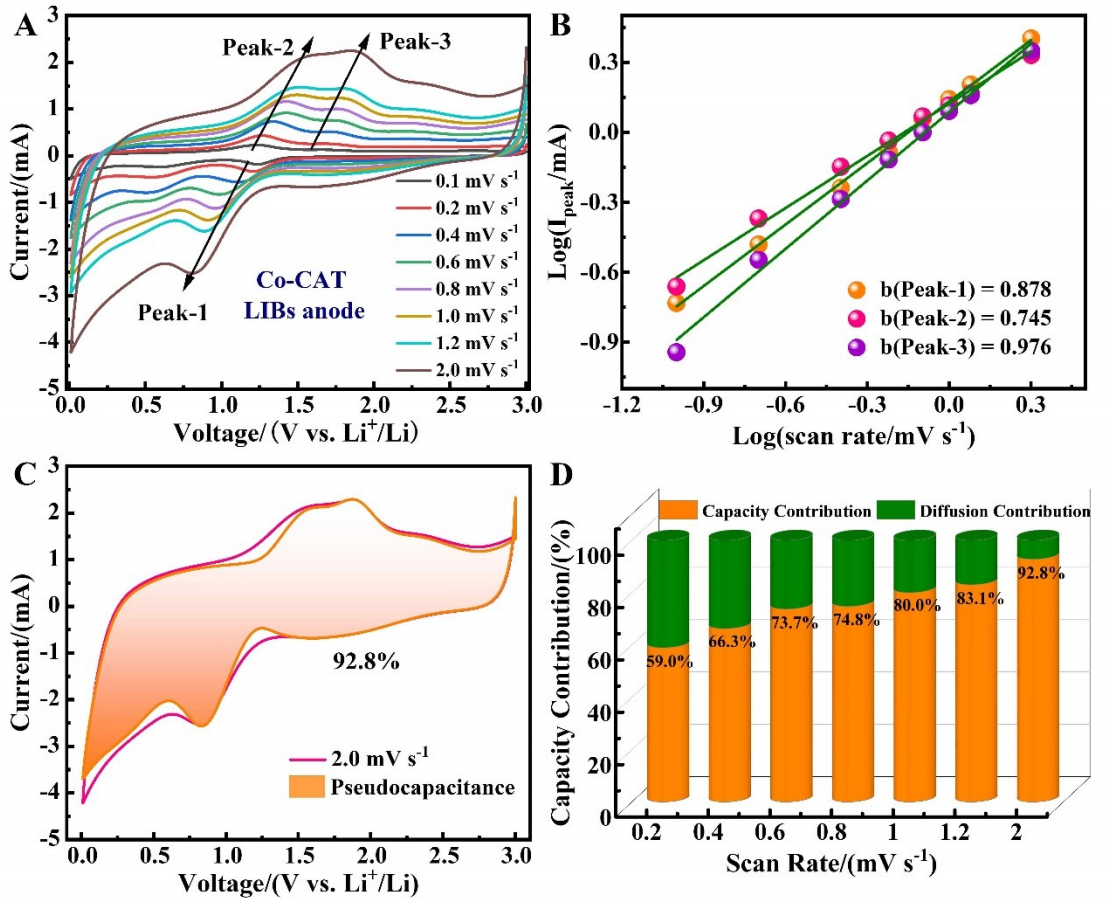

Figure S13. Pseudocapacitive performance of Co-CAT MOF electrode for LIBs. (A) CV profiles of Co-CAT MOF with different scan rates. (B) Relationship between Log(I_{peak}, mA) and Log(scan rate, mV s^{-1}). (C) Contribution of pseudocapacitance (orange region) of Co-CAT MOF electrode at a scan rate of 2.0 mV s^{-1}. (D) Capacity-/Diffusion-contribution ratio of Co-CAT MOF with different scan rates.

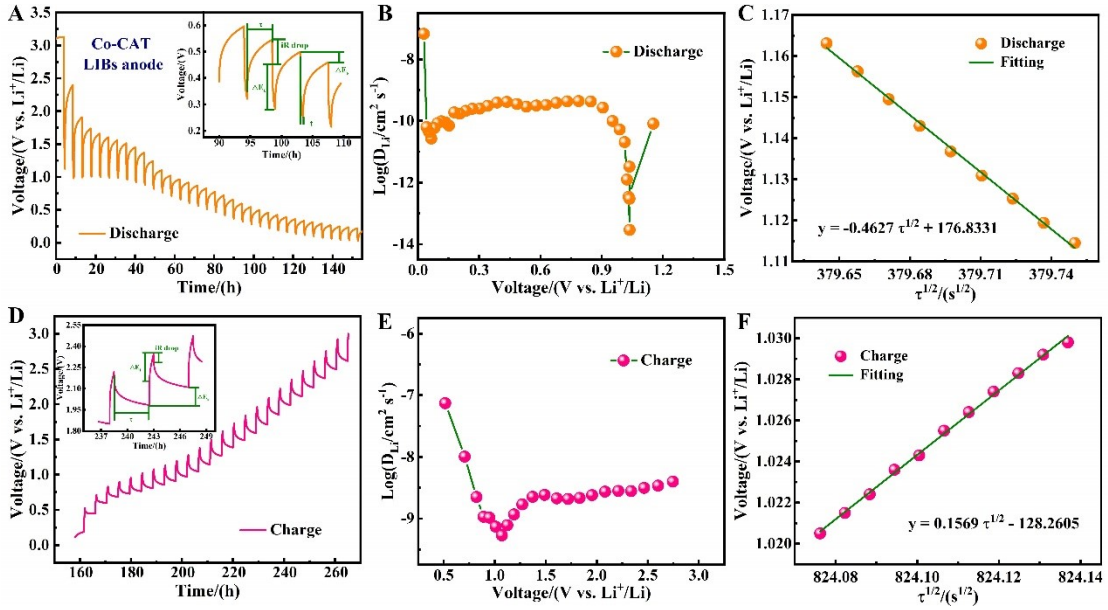

Figure S14. GITT curves of the Co-CAT MOF electrode for the (A) discharge and (D) charge processes in the initial cycle at 100 mA g^{-1}. $\triangle E_s$ and $\triangle E_t$ are the voltage changes caused by pulse discharge and constant current discharge. The variation of D_{Li}^{+} during (B) discharge and (E) charge processes. The corresponding linear behaviour of voltage and $t^{1/2}$ during (C) discharge and (F) charge processes.

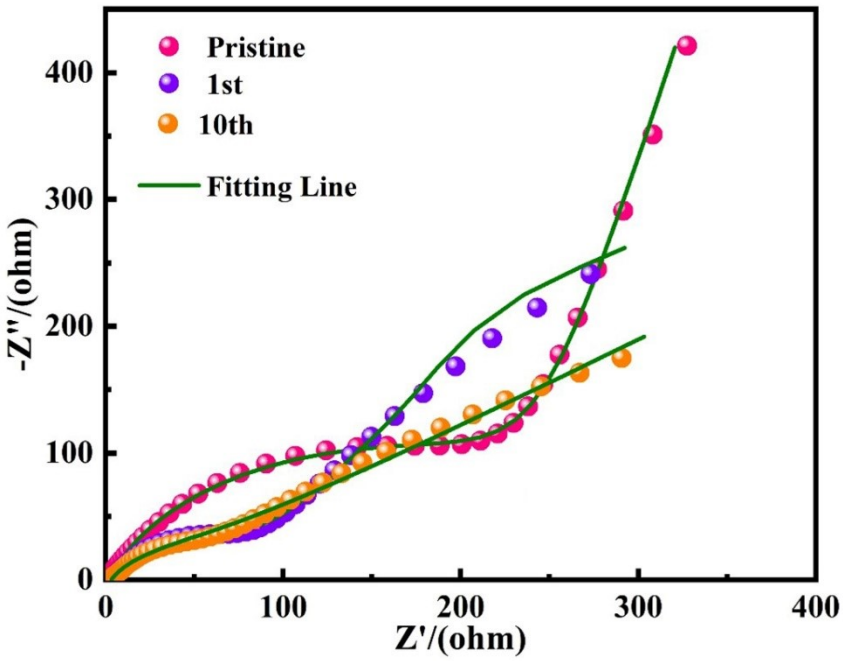

Figure S15. EIS plots of Co-CAT MOF electrodes. With increasing cycles, the radius of the semicircular area decreases, indicating that the reaction kinetics gradually accelerates.

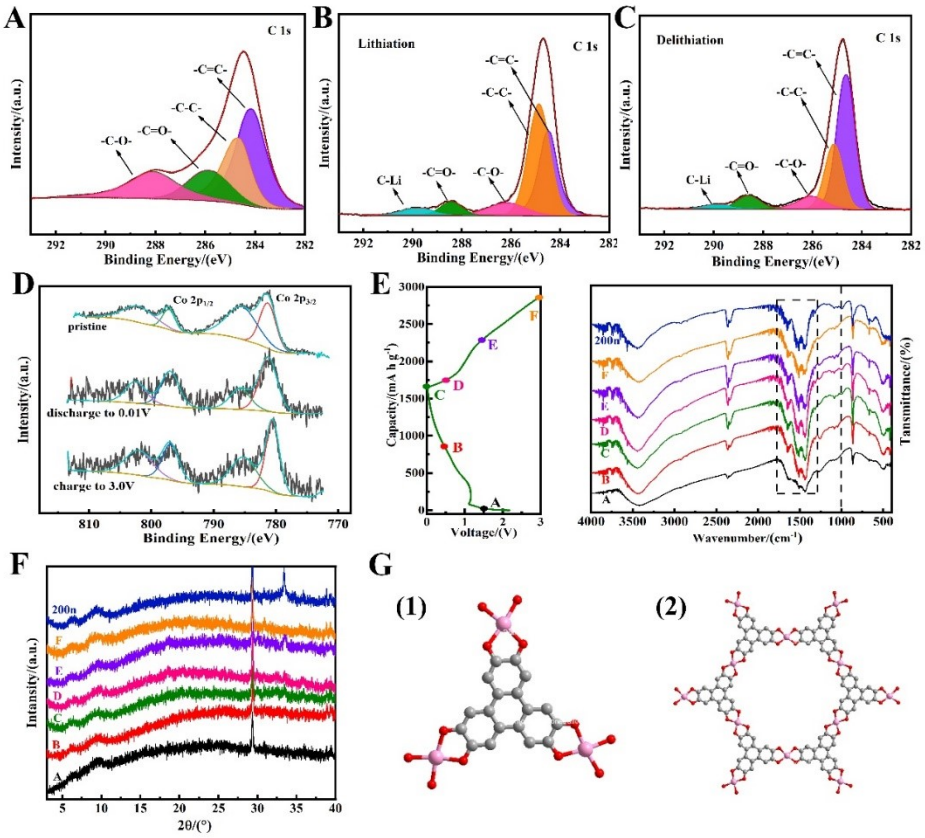

Figure S16. *Ex-situ* characterizations of Co-CAT MOF for LIBs. XPS spectra of C 1s core level: (A) fresh electrode, (B) lithiated electrode, (C) delithiated electrode. (D) XPS spectra of Co 2p region. (E) FTIR curves and (F) *ex-situ* XRD profiles under different charge/discharge status. (G) Potential lithium-ion storage sites of Co-CAT MOF electrode.

Table S1. Comparison of potassium-storage performance of different MOF-based anode materials.

MOFs	Voltage range V vs. K^+/K	Reversible capacity (mA h g^{-1})/cycle number	Current density /(mA g^{-1})	Ref.
K_2TP	0.1-2.0	229/100	200	1
COF-10@CNT	0.01-3.0	288/500	100	2
MOF-235/graphene	0.01-3.0	180/200	200	3
MIL-125(Ti)	0.01-3.0	155/200	50	4
MOF-235/CNT	0.01-3.0	144/50	50	5
$Co_3[Co(CN)_6]_2$	0.05-2.0	324.5/200	100	6
Co-MOF-rGO	0.01-3.0	364/200	200	7
Co-CAT	**0.01-3.0**	**332/80**	**100**	**This**
	0.01-3.0	**280/200**	**500**	**work**
	0.01-3.0	**230/700**	**1000**	

Table S2. Comparison of electrochemical performance of typical Co-based MOF anode materials for LIBs.

MOFs	Voltage range V vs. Li^+/Li	Reversible capacity (mA h g^{-1})/cycle number	Current density /(mA g^{-1})	Ref.
Co-ZIF-67	0.01-3	122/100	100	8
Co-btca	0.01-3	867.4/50	100	9
	0.01-3	802.3/50	200	
	0.01-3	773.9/200	500	
	0.01-3	535.4/400	1000	
$[Co_2(pztc)(H_2O)_6]_n$	0.01-3	815/150	200	10
H-$Co_2(OH)_2$BDC	0.01-3	1345/100	100	11
	0.01-3	828/700	2000	
S-$Co_2(OH)_2$BDC	0.01-3	1021/200	100	12
	0.01-3	601/700	500	
	0.01-3	435/1000	1000	
CoBTC-EtOH	0.01-3	473/500	2000	13
	0.01-3	856/100	100	
Co-CAT	**0.01-3**	**800/200**	**200**	**This work**

4. Supplementary references

[S1] Lei. K, Li. F, Mu. C, Wang. J, Zhao. Q, Chen. C, Chen. J, *Energy Environ. Sci.*, 2017, **10**, 552-557

[S2] Chen. X, Zhang. H, Ci. C, Sun. W, Wang. Y, *ACS Nano*, 2019, **13**, 3600-3607

[S3] Deng. Q, Luo. Z, Liu. H, Zhou. Y, Zhou. C, Yang. R, Wang. L, Yan. Y, Xu. Y, *Ionics*, 2020, **26**, 5565-5573

[S4] An. Y, Fei. H, Zhang. Z, Ci. L, Xiong. S, Feng. J, *Chem. Comm.*, 2017, **53**, 8360-8363

[S5] Deng. Q, Feng. S, Hui. P, Chen. H, Tian. C, Yang. R, Xu. Y, *J. Alloys Compd.,* 2020, **830,** 154714

[S6] Deng. L, Yang. Z, Tan. L, Zeng. L, Zhu. Y, Guo. L, *Adv. Mater.,* 2018, 30, 1802510

[S7] Xiao. P, Li. S, Yu. C, Wang. Y, Xu. Y, *ACS Nano,* 2020, **14**, 10210-10218

[S8] Wang. H, Bai. Y, Jiang. X, Zeng. M, *Appl. Surf. Sci.,* 2021, **546**, 149119

[S9] Luo. Y, Sun. L, Xu. F, Wei. S, Wang. Q, Peng. H, Chen. C, *J. Mater. Sci. Technol.,* 2018, **34**, 1412-1418

[S10] Liu. J, Zhang. L, Li. H, Zhao. P, Ren. P, Shi. W, Cheng. P, *Sci. China Chem.,* 2019, **62**, 602-608

[S11] Chen. L, Yang. W, Wang. J, Chen. C, Wei. M, *Chem. Eur. J.,* 2018, **24**, 13362-13367

[S12] Li. C, Hu. X, Lou. X, Zhang. L, Wang. Y, Amoureux.J.-P, Shen. M, Chen. Q, Hu. B. *J, Mater. Chem. A,* 2016, **4**, 16245-16251

[S13] Li. C, Lou. X, Shen. M, Hu. X, Guo. Z, Wang. Y, Hu. B, Chen. Q, *ACS Appl. Mater. Interfaces,* 2016, **8**, 15352-15360.